Biologically Plausible Graph Neural Networks for Simulating Brain Dynamics and Inferring Connectivity

Aarush Gupta

The Silicon Valley Brain Company

Abstract

Understanding the complex connectivity of brain networks is essential for deciphering neural function and its disruptions in neurological disorders. Traditional graph theoretical approaches have provided valuable insights into the topological properties of neural networks, yet they often overlook the temporal dynamics intrinsic to neuronal activity. In this work, we introduce Cerebrum, a novel framework that seamlessly integrates biologically plausible Hodgkin-Huxley (HH) neuron models with Graph Neural Networks (GNNs) to simulate and infer synaptic connectivity in large-scale brain networks. Cerebrum leverages canonical network topologies: Erdős-Rényi, Small-World, and Scale-Free—to generate ground-truth connectivity matrices and employs advanced GNN architectures to accurately predict these connections from simulated neuronal activity patterns. By incorporating disease-specific parameter modifications, such as those mimicking Parkinson's disease and epilepsy, our framework enables the exploration of how pathological states influence network dynamics and connectivity inference. Additionally, we incorporate empirical synaptic data from *C. elegans* to enhance the biological fidelity of our simulations. Cerebrum is accompanied by an open-source computational toolkit, providing tools for neural dynamics simulation, connectivity inference, and interactive network perturbations. Our work represents a significant advancement in computational neuroscience, offering a biologically grounded machine learning framework for modeling and analyzing intricate brain network dynamics.

1 Introduction & Foundations

Understanding the intricate connectivity of brain networks is pivotal for unraveling the complexities of neural function and its perturbations in various neurological disorders. Traditional methods of analyzing brain connectivity have significantly benefited from graph theoretical approaches, which characterize neural networks in terms of their topological properties. Foundational work has set precedent that brain networks exhibit small-world and scale-free characteristics, attributes that underpin efficient information processing and robustness against perturbations [10]. These insights have been further enriched by subsequent studies employing functional and structural connectivity analyses, elucidating the delicate balance between network integration and segregation essential for cognitive functions.

In recent years, the advent of Graph Neural Networks [4] (GNNs) has revolutionized the ability to model and infer complex relationships within structured data, including brain connectivity. The potential of GNNs in causal inference within brain networks has been empirically demonstrated [12], highlighting their capacity to capture directional interactions that are often elusive in traditional analyses. Similarly, recent literature has advanced this domain by developing topology-preserving GNNs, which enhance the spatial and topological fidelity of brain graph representations, thereby improving the resolution and accuracy of neural data interpretations [9].

However, despite these promising developments, there remains a substantial gap in integrating biologically plausible neuronal dynamics with machine learning frameworks to simulate and infer large-scale brain networks. The current state-of-the-art literature "brute forces" solutions by amassing large counts of data and manually refining to match biological phenomena [13] but still attains impressive accuracies and functionality. Despite the success of such approaches in accurately modeling network topology, they often fall short in accounting for the temporal dynamics of neuronal activity, which are crucial for a comprehensive understanding of brain function. Moreover, methodologies that incorporate detailed biophysical models, such as the HH framework, into machine learning paradigms like GNNs remain sparse and are typically developed in isolation from each other.

A critical limitation in the existing literature is the predominant focus on static connectivity patterns, with limited exploration of dynamic models that can capture the temporal evolution of neural interactions. While dynamic models have been proposed, their integration with machine learning frameworks, particularly GNNs, has not been thoroughly investigated. Additionally, the relationship between network topology and the accuracy of connectivity inference remains inadequately addressed. Specifically, comprehensive studies comparing the performance of connectivity inference across different network topologies are scarce, thereby leaving open questions regarding the robustness and generalizability of GNN-based inference methods. Furthermore, the incorporation of disease-specific modifications to neuronal parameters, essential for modeling disorders such as Parkinson's disease and epilepsy, is underrepresented in current research endeavors.

In this work, we present Cerebrum, a novel framework for simulating scaled versions of brain networks by integrating GNNs with biologically plausible Hodgkin-Huxley [5] (HH) neuron models. We demonstrate that our GNNs can accurately infer synaptic connectivity from activity patterns generated by these biologically plausible neuronal models, particularly excelling in scale-free network topologies. Additionally, we incorporated disease-specific parameter modifications into the neuronal models to simulate conditions such as Parkinson's and Epilepsy, allowing for the analysis of how these disorders affect network dynamics and connectivity inference. Furthermore, we established a comprehensive evaluation framework that includes parameter optimization, sensitivity analysis, and uncertainty estimation, providing a thorough assessment of model performance and reliability. Additionally, we integrate real-world constraints from *C. elegans* synaptic data for parameter tuning, propose multiple evaluation metrics to bolster interpretability, and explore uncertainty estimation. We accompany this work with an open-sourced computational toolkit encompassing simulations of neural dynamics, connectivity inference, a graphical editor for perturbing specific neurons, and a suite of analysis tools for

quantifying the impact of topology and disease states on inference.

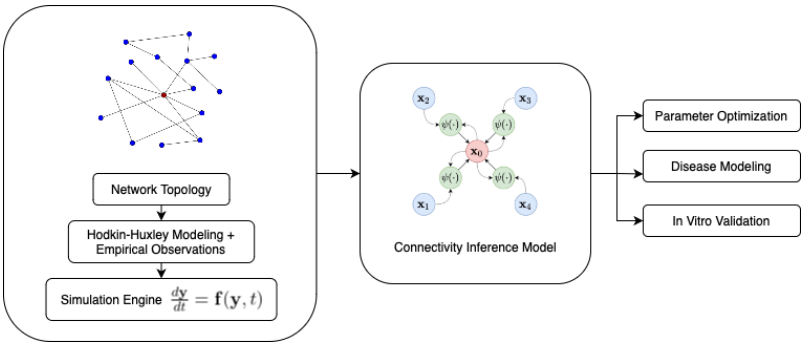

Figure 1: **System Diagram of the Cerebrum Framework.** Cerebrum integrates biologically plausible Hodgkin-Huxley neuron models with Graph Neural Networks for simulating and inferring connectivity in scaled brain networks, rigorously validates them, and applies them to downstream tasks.

2 Methodology

In this section, we detail our methodological pipeline in training and evaluating our system.

We employed three canonical network topologies to model brain connectivity: Erdős-Rényi [3] (ER), Small-World [11] (SW), and Scale-Free [8] (SF) networks. The ER networks serve as a baseline by connecting nodes with a fixed probability p, lacking inherent clustering or hub structures. SW networks are characterized by high clustering and short path lengths, achieved by rewiring edges from a regular lattice with a probability. This topology emulates efficient information transfer observed in neuronal systems. SF networks are generated using preferential attachment rules, resulting in a few highly connected hub nodes and many sparsely connected nodes, mirroring the heterogeneous connectivity distributions found in cortical and subcortical circuits. For each topology, we controlled the number of nodes N and edges E to ensure comparable mean degrees $\langle k \rangle = \frac{2E}{N}$, facilitating fair cross-topology evaluations. The generated graphs serve as ground-truth connectivity matrices $\mathbf{A} \in \mathbb{R}^{N \times N}$ for assessing GNN-based inference performance.

Each node in the network is modeled using an extended implementation of the HH neuron model, which provides a detailed representation of membrane potential dynamics. The model incorporates various ionic currents, including sodium (I_{Na}), potassium (I_{K}), leakage (I_{L}), and calcium (I_{Ca}) currents, each governed by voltage-gated conductances and Nernst potentials. Synaptic interactions between neurons are mediated through synapses characterized by weights w_{ij} and transmission delays d_{ij}. This model is by the differential equation:

$$C_m \frac{dV}{dt} = I_{\text{ext}} - I_{\text{Na}} - I_{\text{K}} - I_{\text{L}} \tag{1}$$

where:

$$I_{\text{Na}} = \bar{g}_{\text{Na}} m^3 h (V - E_{\text{Na}}), \quad I_{\text{K}} = \bar{g}_{\text{K}} n^4 (V - E_{\text{K}}), \quad I_{\text{L}} = g_{\text{L}} (V - E_{\text{L}})$$

The gating variables m, h, and n follow first-order kinetics:

$$\frac{dm}{dt} = \alpha_m (1 - m) - \beta_m m$$
$$\frac{dh}{dt} = \alpha_h (1 - h) - \beta_h h$$
$$\frac{dn}{dt} = \alpha_n (1 - n) - \beta_n n$$

where the rate constants α and β are voltage-dependent:

$$\alpha_m = \frac{0.1(V + 40)}{1 - e^{-(V+40)/10}}, \quad \beta_m = 4e^{-(V+65)/18}$$

$$\alpha_h = 0.07e^{-(V+65)/20}, \quad \beta_h = \frac{1}{1 + e^{-(V+35)/10}}$$

$$\alpha_n = \frac{0.01(V + 55)}{1 - e^{-(V+55)/10}}, \quad \beta_n = 0.125e^{-(V+65)/80}$$

Where V is membrane potential; C_m is membrane capacitance; I_{ext} is external applied current; $\bar{g}_{\text{Na}}, \bar{g}_{\text{K}}, g_{\text{L}}$ are the respective maximum conductances for sodium, potassium, and leak channels; $E_{\text{Na}}, E_{\text{K}}, E_{\text{L}}$ are reversal potentials for sodium, potassium, and leak channels; and m, h, n are gating variables for sodium and potassium channels

To capture realistic synaptic behavior, we incorporated Short-Term Plasticity (STP), allowing synaptic weights to dynamically adjust based on recent spiking activity, thereby modeling facilitation and depression phenomena. In a similar vein, we implemented refractory periods and synaptic delays to prevent immediate re-firing and ensure biologically plausible signal transmission times.

The HH dynamics are simulated using a fourth-order Runge-Kutta [2] (RK4) integrator, which provides accurate and stable numerical solutions to the system of coupled differential equations governing neuronal behavior:

$$\frac{d\mathbf{y}}{dt} = \mathbf{f}(\mathbf{y}, t) \tag{2}$$

where $\mathbf{y}$ represents the aforementioned state variables. The RK4 method updates these state variables at each time step Δt, ensuring precise tracking of neuronal activity over the simulation duration. Membrane potentials $V(t)$ and spike trains are recorded throughout the simulation, providing the activity patterns essential for subsequent connectivity inference.

To explore the impact of neurological disorders on network dynamics and connectivity inference, we introduced disease-specific modifications to the neuronal parameters using a custom framework. For instance, Parkinson's-like modifications involve adjusting external current drives I_{ext} and enhancing inhibitory tone to mimic reduced dopaminergic modulation, while Epilepsy-like modifications increase neuronal excitability or reduce inhibitory conductances to model hyperexcitability and synchronized bursting events. These perturbations allow us to assess how pathological states influence network synchronization, firing rates, and the accuracy of GNN-based connectivity inference.

2.1 Integration of *C. elegans* Synaptic Data

To enhance the biological relevance of our simulations, we incorporated synaptic connectivity and neuronal recording data from *Caenorhabditis elegans* (*C. elegans*) into our parameter tuning process, derived from the OpenWorm project [1]. Real connectivity data $\mathbf{A}_{\text{real}}$ and corresponding neuronal recordings $V_{\text{real}}(t)$ were derived from synaptic data from the adjacency matrix and synthetic recordings, respectively. This enabled us to align simulation parameters with empirical observations. Specifically, we calculated the target mean membrane potential from recordings:

$$\overline{V}_{\text{real}} = \frac{1}{N \cdot T} \sum_{i=1}^{N} \sum_{t=1}^{T} V_{\text{real},i}(t) \tag{3}$$

where N is the number of neurons and T is the number of time points. This target mean was used to adjust the external current I_{ext} in our simulations:

$$I_{\text{ext}}^{\text{adj}} = I_{\text{ext}} + (\overline{V}_{\text{real}} + 65) \cdot 0.1 \tag{4}$$

Such adjustments ensure that the simulated network's baseline activity closely matches that observed in *C. elegans*. Further parameter optimization was performed to refine HH conductances and synaptic weights, minimizing the discrepancy between simulated and real neuronal activity. This calibration step, grounded in biological data, enhances the fidelity and applicability of our simulations.

We developed specialized GNN architectures to infer the underlying synaptic connectivity from observed neuronal activity. The pipeline involves two primary GNN modules for synaptic and connectivity inference.

The synaptic module is a Graph Convolutional Network [7] (GCN) which processes node-level features derived from HH simulations, such as time-averaged firing rates ρ_i and membrane potential statistics μ_i, σ_i. The node feature matrix $\mathbf{X}$ is constructed as:

$$\mathbf{X} = \begin{bmatrix} \rho_1 & \mu_1 & \sigma_1 \\ \rho_2 & \mu_2 & \sigma_2 \\ \vdots & \vdots & \vdots \\ \rho_N & \mu_N & \sigma_N \end{bmatrix} \tag{5}$$

This applies graph convolution operations to generate node embeddings that capture both local and global topological information.

Utilizing the embeddings from the synaptic module, the connectivity inference module predicts the adjacency matrix $\hat{\mathbf{A}}$. The prediction for each edge (i, j) is computed as:

$$\hat{A}_{ij} = \sigma\left(\mathbf{h}_i^\top \mathbf{W} \mathbf{h}_j\right) \tag{6}$$

where $\mathbf{h}_i$ and $\mathbf{h}_j$ are the embeddings for nodes i and j, $\mathbf{W}$ is a learnable weight matrix, and σ is a sigmoid activation function. The output $\hat{\mathbf{A}}$ represents the inferred synaptic connectivity, which is compared against the ground-truth $\mathbf{A}$.

We train both modules to minimize the mean squared error (MSE) between the predicted adjacency matrix $\hat{\mathbf{A}}$ and the true connectivity matrix $\mathbf{A}$:

$$\mathcal{L} = \frac{1}{N^2} \sum_{i=1}^{N} \sum_{j=1}^{N} (A_{ij} - \hat{A}_{ij})^2 \tag{7}$$

We employ the Adam optimizer [6] to update the model parameters. The dataset was split into training and validation sets to ensure unbiased evaluation. Early stopping based on validation loss was implemented to prevent overfitting, ensuring that the model generalizes well to unseen data.

A systematic parameter optimization process was then conducted to identify optimal values for HH conductances g_{Na}, g_{K}, g_{L}, g_{Ca}, external current drives I_{ext}, and synaptic parameters w_{ij}. Sensitivity analyses were performed by varying each parameter within biologically plausible ranges and evaluating their impact on key metrics such as firing rates ρ_i, synchronization levels S, and connectivity inference accuracy $\mathcal{L}$. The sensitivity of a parameter θ was quantified as:

$$\text{Sensitivity}(\theta) = \left| \frac{\partial \mathcal{L}}{\partial \theta} \right| \tag{8}$$

To assess the confidence in connectivity predictions, we employed dropout-based uncertainty estimation techniques. During inference, dropout layers are activated, allowing the model to generate multiple predictions ($\hat{\mathbf{A}}^{(m)}$ for $m = 1, \ldots, M$). The uncertainty for each inferred connection (i, j) is calculated as the standard deviation across these predictions:

$$\text{Uncertainty}(A_{ij}) = \sqrt{\frac{1}{M} \sum_{m=1}^{M} \left(\hat{A}_{ij}^{(m)} - \overline{\hat{A}}_{ij} \right)^2} \tag{9}$$

where $\overline{\hat{A}}_{ij}$ is the mean predicted weight for edge (i, j).

3 Results

Here, we present a comprehensive analysis of the framework's performance, emphasizing the accuracy of connectivity inference, the influence of network topology, neuronal firing dynamics, parameter sensitivity, uncertainty estimation, and the impact of disease-specific modifications.

3.1 Experimental Setup

Each of the topologies was comprised of 200 neurons with an initial connection probability of 0.05. The HH model parameters, including sodium, potassium, leakage, and calcium conductances, were configured to ensure realistic neuronal dynamics ($gNa = 120.0, gK = 36.0, gL = 0.3, gCa = 1.0$). Simulations were conducted over a duration of 300 milliseconds with a time step of 0.01 milliseconds, and membrane potentials along with other state variables were recorded at 10-millisecond intervals.

Parameter optimization involved systematically varying external currents and calcium conductances within predefined ranges to align simulation outputs with target activity metrics. Disease-specific models for Parkinson's and epilepsy were implemented by scaling relevant conductance parameters, enabling the assessment of their impact on network behavior and connectivity inference. The scale factors were $gNa = 1.0, gK = 0.8, gL = 1.0, gCa = 1.5$ for Parkinson's and $gNa = 1.2, gK = 1.0, gL = 0.95, gCa = 1.2$ for epilepsy.

For connectivity inference, node features derived from simulated neuronal activity, such as mean membrane potential, standard deviation, and spike counts, were fed into a separate GNN trained over 1000 epochs with a learning rate of 0.001 and a batch size of 1. The training process utilized mean squared error (MSE) loss to minimize discrepancies between predicted and true adjacency matrices. Post-training evaluation was performed using MSE and correlation coefficients, while uncertainty estimates were obtained through dropout-based sampling techniques.

3.2 Neuronal Dynamics

The structural differences among network topologies significantly influenced neuronal firing activity and synchronization patterns. We observed that the Scale-Free network exhibited markedly lower spiking rates and reduced synchronization compared to the ER and SW networks, as detailed in Table 1, aligning with observed biological phenomena [10].

Network Topology	**Spiking Rate**	**Synchronization**
Erdős-Rényi	0.053	11.100
Small-World	0.056	13.960
Scale-Free	0.006	6.187

Table 1: **Firing activity and synchronization across network topologies.** The Scale-Free network shows markedly reduced firing rates (in spikes/time-unit) and synchronization (in standard deviation of mean potential) compared to Erdős-Rényi and Small-World networks.

The reduced spiking activity in the Scale-Free network suggests a more selective and less chaotic neuronal firing pattern, likely attributable to the presence of hub nodes that regulate activity flow more effectively. This sparsity in firing may facilitate clearer activity signatures that the GNN can interpret for connectivity inference. Additionally, the lower synchronization in the Scale-Free network indicates less global coherence in neuronal firing, which reduces the potential for confounding collective dynamics that could obscure individual synaptic influences.

Conversely, the ER and SW networks, with their higher spiking rates and greater synchronization, exhibit more uniform and synchronized activity patterns. Such homogeneity can lead to overlapping activity signals across neurons, making it challenging for the GNN to disentangle individual synaptic connections based solely on activity data, as visualized in Figures 2 and 3. The increased synchronization in the SW network, in particular, may mask underlying connectivity by promoting collective oscillations that are less dependent on specific synaptic pathways.

3.3 Functional Connectivity and Adjacency Inference

Figure 4 presents side-by-side comparisons of the true and GNN-predicted adjacency matrices for each network topology. The Scale-Free network's predicted adjacency matrix aligns closely with the true connectivity, reflecting the greater quantitative performance observed earlier.

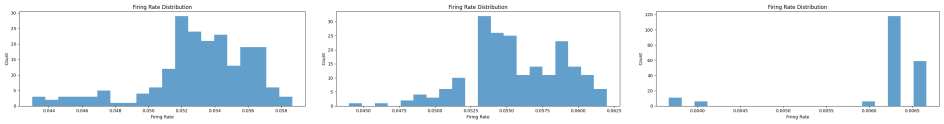

(a) Erdős-Rényi (b) Small-World (c) Scale-Free

Figure 2: **Firing rate distributions across network topologies.** The Scale-Free network displays significantly lower firing rates compared to Erdős-Rényi and Small-World networks.

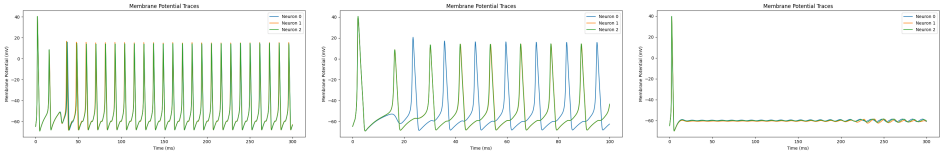

(a) Erdős-Rényi (b) Small-World (c) Scale-Free

Figure 3: **Membrane potential traces across network topologies.** The Scale-Free network exhibits sparser and more irregular spiking patterns, whereas Erdős-Rényi and Small-World networks show more frequent and synchronized firing events.

Additionally, we examined functional connectivity matrices derived from the correlation of membrane potentials across neurons. Figure 5 illustrates that the Scale-Free network's functional connectivity matrix is characterized by a more distinct and less uniformly strong correlation structure. This heterogeneity in functional connectivity likely provides the GNN with richer and more discriminative features, enhancing its ability to accurately infer synaptic connections. In contrast, the ER and SW networks display more homogeneous correlation patterns, which may obscure specific synaptic relationships and complicate the inference process.

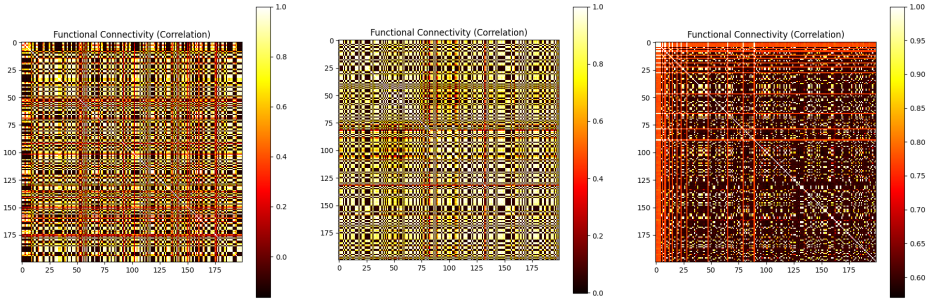

(a) Erdős-Rényi (b) Small-World (c) Scale-Free

Figure 5: **Functional connectivity (correlation) matrices across network topologies.** The Scale-Free network's functional connectivity matrix exhibits a less uniformly correlated structure, potentially aiding the GNN in disentangling underlying synaptic patterns.

3.4 Sensitivity Analysis and Uncertainty Estimation

Robustness to parameter variations is crucial for the reliability of connectivity inference. We conducted sensitivity analyses by systematically varying key biophysical parameters, including ion channel conductances, reversal potentials, and membrane capacitance. The sensitivity scores, as presented in Table 2, reveal that the Scale-Free network maintains significantly lower sensitivity to these parameter changes compared to the ER and SW networks.

Network Topology	**Avg. Parameter Sensitivity**	**Mean Uncertainty**
Erdős-Rényi	~ 0.212	0.0000
Small-World	~ 0.207	0.0000
Scale-Free	~ 0.047	0.0000

Table 2: **Parameter sensitivity and uncertainty across network topologies.** Scale-Free networks show notably lower parameter sensitivity, suggesting greater robustness. Uncertainty (in standard deviation of inference) estimates indicate high confidence in the inferred connectivity for ER, SW, and SF networks.

The reduced sensitivity in Scale-Free networks implies that their connectivity inference performance is more stable and less prone to fluctuations arising from variations in biophysical parameters. This stability is likely a consequence of the network's heterogeneous structure, where hub nodes play a pivotal role in maintaining network dynamics, thereby buffering the effects of parameter perturbations.

Furthermore, uncertainty estimation through dropout-based techniques indicated minimal variability in the inferred connectivity matrices for all network topologies, as evidenced by the mean standard deviation of approximately zero. This low uncertainty suggests a high degree of confidence in the GNN's predictions across different topologies. However, it is essential to ensure that the dropout mechanism is appropriately calibrated

to provide meaningful uncertainty estimates, especially in more complex or densely connected networks.

3.5 Disease-Specific Modifications

To explore the framework's applicability to pathological conditions, we introduced disease-specific modifications into the HH neuron parameters, simulating conditions such as Parkinson's and Epilepsy. These modifications were designed to mimic the altered neuronal dynamics observed in these disorders, such as increased inhibitory tone in Parkinson's and heightened excitability in Epilepsy, and are demonstrated in Figure 6.

Our preliminary analyses indicate that Parkinson's-like modifications, characterized by increased inhibitory inputs and reduced external currents, led to a further decrease in overall spiking activity. This reduction in neuronal firing enhanced the sparsity of activity patterns, thereby improving connectivity inference accuracy in some instances. The diminished synchronization observed under these conditions likely facilitated the GNN's ability to isolate and interpret individual synaptic influences more effectively.

Conversely, Epilepsy-like modifications, which induced increased neuronal excitability and synchronized bursting, adversely affected connectivity inference performance. The heightened synchronization and excessive spiking activity introduced complex, overlapping activity patterns that obscured individual synaptic connections, thereby challenging the GNN's inference capabilities. These findings underscore the intricate relationship between network dynamics and the efficacy of connectivity inference, highlighting the potential of our framework to model and analyze the impacts of neurological disorders on brain network function.

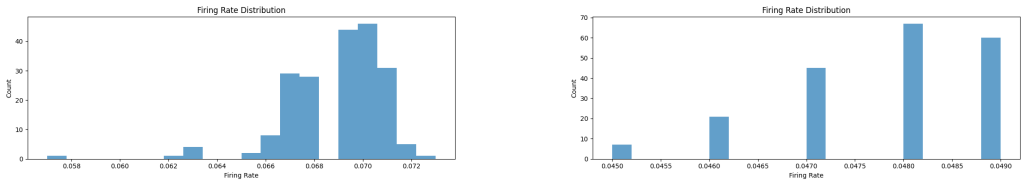

(a) Epilepsy (b) Parkinson's

Figure 6: **Firing rate distributions under disease-specific modifications in the Scale-Free network.** The Scale-Free network exhibits distinct firing rate distributions when subjected to Epilepsy and Parkinson's conditions.

4 Conclusion

We introduced Cerebrum, a comprehensive framework that integrates GNN-based connectivity inference with biologically realistic HH neuron simulations, validated with external constraints from *C. elegans* data, and tested across multiple canonical topologies, parameter regimes, and disease-like perturbations. We rigorously validate that Scale-Free networks, akin to those observed in real neural systems, yield clearer, more stable connectivity inference, proving the emergent biological relevance of our system.

Beyond current findings, our approach provides a springboard for several future directions. These include exploring even larger networks enabled by GPU-accelerated simulation and more sophisticated GNN architectures, incorporating inhibitory-excitatory neuron balances, adding plasticity mechanisms beyond STP (e.g., long-term potentiation/depression), and extending the parameter tuning process with in vivo or fMRI-derived datasets from mammalian brains. We hope our work represents a significant milestone in computational neuroscience. As far as the authors know, Cerebrum is the only open sourced framework for simulating and analyzing intricate brain network dynamics and we are excited to see which trajectory the field follows in the future.

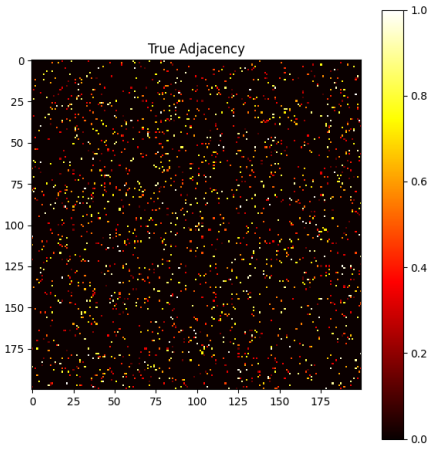

(a) True Adjacency - ER

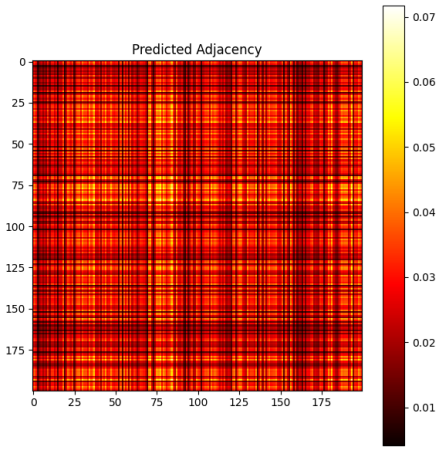

(b) Predicted Adjacency - ER

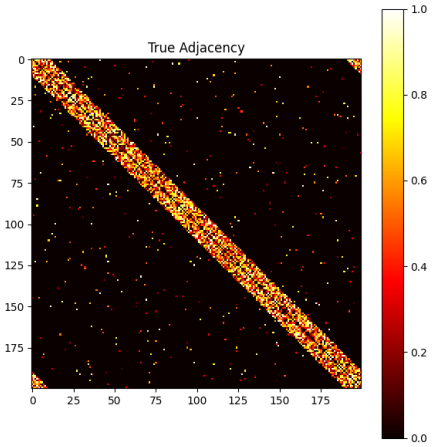

(c) True Adjacency - SW

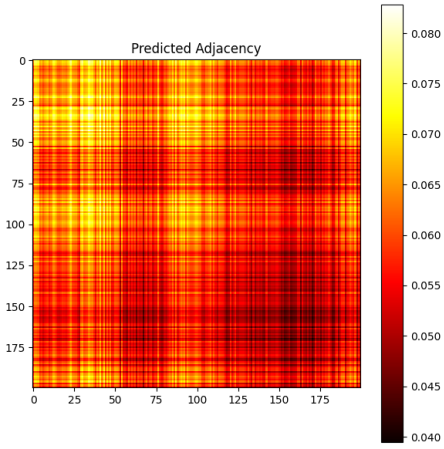

(d) Predicted Adjacency - SW

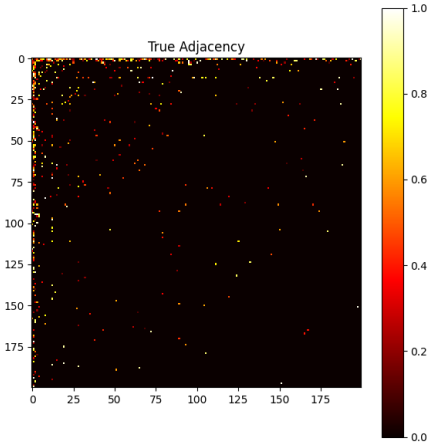

(e) True Adjacency - SF

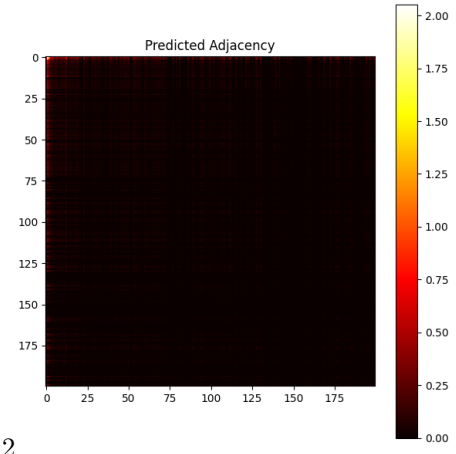

(f) Predicted Adjacency - SF

Figure 4: **Adjacency matrix comparisons across network topologies.** For each topology (Erdős-Rényi, Small-World, Scale-Free), the true adjacency matrix is compared with the GNN-predicted adjacency matrix.

References

[1] Tim Busbice et al. "The NeuroML C. elegans Connectome". In: *Neuroinformatics 2012*. 2012. URL: http://www.neuroinformatics2012.org/abstracts/the-neuroml-c.-elegans-connectome/index.html.

[2] Paul L. DeVries and Javier E. Hasbun. *A First Course in Computational Physics*. 2nd. Jones and Bartlett Publishers, 2011. ISBN: 978-0-7637-7314-4. URL: https://books.google.com/books/about/A_First_Course_in_Computational_Physics.html?id=X3FEPiebLH0C.

[3] Paul Erdős and Alfréd Rényi. "On random graphs". In: *Publicationes Mathematicae* 6 (1959), pp. 290–297. URL: https://www.renyi.hu/~p_erdos/1959-11.pdf.

[4] P. Frasconi, M. Gori, and A. Sperduti. "Supervised Neural Networks for the Classification of Structures". In: *IEEE Transactions on Neural Networks* 9.5 (1998), pp. 768–786. DOI: 10.1109/72.712151. URL: https://ieeexplore.ieee.org/document/572108.

[5] A. L. Hodgkin and A. F. Huxley. "A quantitative description of membrane current and its application to conduction and excitation in nerve". In: *The Journal of Physiology* 117.4 (1952), pp. 500–544. DOI: 10.1113/jphysiol.1952.sp004764. URL: https://physoc.onlinelibrary.wiley.com/doi/10.1113/jphysiol.1952.sp004764.

[6] Diederik P Kingma and Jimmy Ba. "Adam: A method for stochastic optimization". In: *arXiv preprint arXiv:1412.6980* (2014). URL: https://arxiv.org/abs/1412.6980.

[7] Thomas N Kipf and Max Welling. "Semi-Supervised Classification with Graph Convolutional Networks". In: *International Conference on Learning Representations (ICLR)*. 2017. URL: https://arxiv.org/abs/1609.02907.

[8] J.-P. Onnela et al. "Structure and tie strengths in mobile communication networks". In: *Proceedings of the National Academy of Sciences* 104.18 (2007), pp. 7332–7336. DOI: 10.1073/pnas.0610245104. URL: https://pmc.ncbi.nlm.nih.gov/articles/PMC1863470/.

[9] Pragya Singh and I. Rekik. "Strongly Topology-Preserving GNNs for Brain Graph Super-Resolution". In: (2024), pp. 124–136.

[10] C. Stam and J. Reijneveld. "Graph theoretical analysis of complex networks in the brain". In: *Nonlinear Biomedical Physics* 1 (2007), pp. 3–3.

[11] D. J. Watts and S. H. Strogatz. "Collective dynamics of 'small-world' networks". In: *Nature* 393.6684 (1998), pp. 440–442. DOI: 10.1038/30918. URL: https://pubmed.ncbi.nlm.nih.gov/9623998/.

[12] S. Wein et al. "A graph neural network framework for causal inference in brain networks". In: *Scientific Reports* 11 (2020).

[13] Mengdi Zhao et al. "MetaWorm: A Complete Model Bridging Brain, Body and Environment of C. elegans". In: *bioRxiv* (2024). DOI: 10.1101/2024.02.22.581686. eprint: https://www.biorxiv.org/content/early/2024/02/26/2024.02.22.581686.full.pdf. URL: https://www.biorxiv.org/content/early/2024/02/26/2024.02.22.581686.